Structural Properties of Ammonium Perchlorate Compressed to 5.6 GPa

Suhithi M. Peiris,*,†,§ G. I. Pangilinan,†,‡,§ and T. P. Russell†,§

High-Energy Materials Section, Code 6112, Chemistry Division, Naval Research Laboratory, Washington, DC 20375, and Nova Research Inc., Alexandria, Virginia 22308

Received: June 16, 2000; In Final Form: September 19, 2000

The effect of pressure to 5.6 GPa on the structure of ammonium perchlorate (AP, NH_4ClO_4) was investigated at room temperature using X-ray diffraction studies and IR and Raman spectroscopy. Two phase transitions were observed. Under hydrostatic conditions, the first transition starts at about 0.9 GPa with the appearance of a few new diffraction peaks and a discontinuity in the pressure-induced shifts of certain Raman frequencies. This transition is most likely a molecular change in AP due to "freezing" of freely rotating NH_4 units, similar to effects at low temperature. The second transition starts at 2.9 GPa with a drop in diffraction intensity followed by a new pattern of diffraction peaks by 3.0 GPa. This transition is also characterized by another discontinuity in the Raman shifts and the emergence of two new Raman modes. The phase above 3.0 GPa is stable to 5.6 GPa. The P−V data to 0.9 GPa obtained from X-ray diffraction measurements were used to calculate a bulk modulus of 15.2 ± 0.3 GPa for the ambient-pressure phase.

I. Introduction

Ammonium perchlorate (NH_4ClO_4, or AP) is the most widely used energetic material. Unfortunately, AP is also one of the least understood energetic materials. Over the past several decades numerous papers have been devoted to the decomposition mechanism and structural properties of AP. The decomposition of AP is rather complicated; mainly because this simple molecule consists of 4 different elements—N, H, Cl, and O. If one considers all the potential oxidation states of these 4 elements, over 1000 possible chemical reactions can be written for the decomposition of AP. In addition, what makes AP completely different from other propellant and explosive ingredients is the presence of chlorine. Most, if not all, other energetic materials consist of only carbon, hydrogen, nitrogen, and oxygen. (Exceptions to this are the recently developed organic difluoramino structures.) Furthermore, impurities play a significant role in the decomposition, combustion, and burn rate of AP materials. Because of these complications the reaction chemistry of AP is still largely not understood. An excellent review elucidating the current theories on decomposition and combustion of AP has been recently compiled.[1]

One fundamental aspect of AP decomposition and burning is the structure of AP during a high-pressure explosion. The structural properties of AP at pressure are not well characterized. At ambient pressure and temperature, AP is an orthorhombic structure with the ClO_4^- ions locked into particular orientations while the NH_4^+ ions rotate freely through a span of orientations within their lattice sites.[2] During heating, around 238 °C the orthorhombic lattice expands and forms a cubic structure just prior to, or during, decomposition. The cubic structure is stabilized by almost-unrestricted rotational reorientation of the perchlorate ions.[3] During further heating these ClO_4^- ion rotations then destabilize the crystal lattice and AP is thought to partially liquefy, forming neutral NH_3 and $HClO_4$ molecules in the condensed phase.[4] During cooling of AP from room temperature down, opposite effects are observed. The free rotation of the ammonium ion is slowly quenched to smaller rotations, then to rocking motions, and finally to what is essentially definitive orientations. A detailed description of this phenomenon is still not available. A recent neutron diffraction study at 298, 78, and 10 K describes the "free rotations" of the NH_4^+ ion as very-large-amplitude rotational oscillations about a definite equilibrium position but doubt the presence of structural phase transitions between 10 and 298 K.[4] However, a detailed Raman study observes two anomalous changes in line widths and frequency shifts, one at about 180 K and another at about 40 K, suggesting phase transitions.[5] They publish that cooling below 180 K promotes the formation of hydrogen bonds which in turn distorts NH_4^+ ions and restricts their motions while ClO_4^- ions are relatively undisturbed. Further cooling below 40 K, however, is said to result in a transformation involving the reordering of both ions.

Even less is known about the structural behavior of AP as pressure is increased. In fact, the few papers on high-pressure studies of AP report many discrepancies. These discrepancies indicate the complexity and incomplete understanding of the structural properties of AP. Therefore, this paper focuses on a detailed study of the structural properties of AP as a function of pressure. Our results indicate the existence of two transitions, which help eliminate many of the previous discrepancies. These new results, when compared and combined with previous reports, support the development of a single concise and complete picture of the high-pressure structural properties of AP.

II. Background

Bridgman reported the first high-pressure study on AP and observed a cusp-like maximum at 3.1 GPa using shear experiments at elevated temperature.[6] The change in volume due to this transition was reported to be too small to quantify. Later, X-ray diffraction measurements with isothermal compression were recorded up to 5.0 GPa.[7] This work was combined with a

* Author to whom correspondence should be addressed.
† Naval Research Laboratory.
‡ Nova Research Inc.
§ Current address: Chemistry and Detonics Division, Code 920, Naval Surface Warfare Center—Indian Head, 101 Strauss Ave., Indian Head, MD 20640.

10.1021/jp002168c CCC: $19.00
Published on Web 11/03/2000

shock compression study of the bulk sound speed. During isothermal compression, five diffraction patterns at pressures of 1.33, 1.34, 2.80, 3.14, and 3.57 GPa indicated no discernible lattice changes. However, by 4.70 GPa some changes in the diffraction pattern were observed indicating a new phase.[7] Unfortunately, it was not possible to solve this diffraction pattern, but it is reported that this pattern was characteristic of an asymmetrical structure such as triclinic or monoclinic. In addition, infrared spectroscopy has been used to study the structure of AP as a function of pressure.[8] The disappearance of the ν_1 ClO_4 band (at 939 cm^{-1}) between 1.0 and 2.4 GPa indicated a possible phase transformation. These researchers speculate that the new phase could be a cubic phase.

As described, three independent groups have observed high-pressure phase transitions in AP albeit at different pressures, ranging from 1.0 to 4.7 GPa. Furthermore, the high-pressure structure has been identified as triclinic, monoclinic, or cubic. To further complicate AP structural properties as a function of pressure, an optical study of the compression of AP was performed.[9] They report no evidence of high-pressure phase transitions up to 26 GPa. However, this work does report the pressure dependence of the orthorhombic−cubic phase transition at high temperature and the pressure dependence of the solid−liquid transition.

Clearly, the high-pressure structural properties of AP are not even remotely understood at this time. Our experiments were designed with the intention of clarifying the ambiguities in these reports and focused on the high-pressure phases of AP at room temperature. Our results when compared and combined with previous reports of the behavior of AP at both high pressures and low temperatures, begin to provide a single concise and complete picture of the pressure/temperature phase diagram of AP. In this study the structural properties of AP were investigated using infrared spectroscopy, Raman spectroscopy, and energy-dispersive X-ray diffraction. In addition, we used our P−V data obtained from the X-ray diffraction experiments to calculate the isothermal bulk moduli of AP at room temperature. The values obtained, and the equation of state fits, will be used to comment on the effect of the phase transitions on the thermodynamic parameters of AP.

III. Experimental Method

A. Materials. AP samples were obtained by cleaving large crystals of AP (approximately $1'' \times 1'' \times 1/2''$) obtained from Dr. T. Boggs of the Naval Weapons Center in China Lake, CA. This AP was used without further purification. The samples used in the experiments described below were prepared as necessary for each particular experimental method. When single crystals are indicated, single crystals cleaved from the large crystals were used. When powders were required, AP crystals were finely ground in a mortar and pestle in to a pure AP powder, or mixed with NaCl in a AP:NaCl ratio of 4:1.

B. Infrared and Raman Spectroscopy. Infrared spectra were collected on a Nicolet 800 FTIR spectrometer, employing an MCT-A detector for improved sensitivity. Typical spectra were obtained by collecting 500 scans of the interferometer with the parameters set at 1 cm^{-1} resolution. Infrared spectra were collected on pure powdered AP samples loaded and compressed to a thin sheet (approximately 5−7 μm thick) between two NaCl windows. A small ruby sphere (10 μm) was placed inside the NaCl to measure the pressure. Spectra were collected at 0.1 GPa pressure increments.

Raman spectra were collected on a Spex 1403 double monochromator employing a Spectrum One liquid-nitrogen-cooled charge-coupled device detector. A Spectra Physics Ar^+ ion laser operating at 514.5 nm at a power of 300 mW focused to a 100-μm diameter spot was used. Raman scatter was collected with high resolution (1 cm^{-1} band-pass) at 0.1 GPa pressure increments to discern subtle changes. Peak positions were determined by fitting Gaussian functions to the observed Raman vibrational peaks.

Raman samples consisted of AP single crystals cleaved or sliced, and suitably sized to fit within the gasket hole with sufficient space for true hydrostatic compression. A small ruby sphere (10 μm in diameter) was added to each sample (to measure pressure) and the gasket hole was filled with FC-75 ($C_8F_{16}O$) as a pressure medium. FC-75, a fluorocarbon liquid, was used as a pressure medium because it retains hydrostaticity to 3.5 GPa, has a slower evaporation rate than most of the methanol−ethanol solutions traditionally used, and is significantly less reactive than organic solvents. A few samples were also prepared without a pressure-transmitting medium to study the effect of non-hydrostaticity.

The high-pressure cell used for spectroscopic studies replicated the NIST clamped anvil-cell design. This cell is fabricated from a high temperature, high-strength Inconel 718 alloy and is designed for reflection and transmission measurements. Two types of anvils (diamond and sapphire) were used in these studies.[10] The diamonds, purchased in the 8-facet anvil cut from Harris Diamonds Inc., weighed a 0.5 carat each with the culets polished to 0.7 mm flats. The sapphire anvils were prepared from brilliant-cut gem-quality sapphires purchased commercially. Each stone weighed 0.3 carats and the culet tips were polished to 0.5−0.6 mm flat surfaces. Tantalum gaskets were used to contain the sample. These were cut out of 0.2 mm thick Ta sheets and drilled with 0.3−0.5 mm diameter gasket holes. The NIST high-pressure cell was mounted on a micrometer-positioning device for alignment.

Pressures were measured by the ruby fluorescence technique.[11] An Ar^+ laser operating at 514.5 nm with a continuous wave power of 100 mW was used to excite the ruby fluorescence R lines. The focused laser beam was 100 μm in diameter. The measured pressures are accurate to 0.05 GPa when hydrostatic pressure conditions are maintained. The uncertainty in the pressure measurement is larger, approximately 0.15 GPa, for the IR measurements because of the absence of a pressure-transmitting medium and therefore non-hydrostatic conditions.

The laser fluence used for both Raman and ruby pressure measurements was lower than the fluence reported to heat the sample and the ruby pressure sensor. The sample temperature was measured by a chromel−alumel thermocouple with its bead in contact with the gasket, to monitor temperature.

C. X-ray Diffraction. Energy-dispersive X-ray diffraction experiments were carried out at the B1 line of the Cornell High Energy Synchrotron Source (CHESS). The solid-state Ge detector was calibrated using the K_α, K_β lines of Mn, Cs, and Ba, and set at a 2θ angle of either 9° or 12°. X-ray diffraction patterns were collected for 12−20 min at each pressure. The energy (E) of each diffraction peak was estimated by fitting a Gaussian function to the peak. The corresponding d-space (d) was calculated by applying $E = h\nu = hc/\lambda$, where $\lambda = 2d \sin\theta$ from Bragg's Law. Each diffraction pattern consisted of 15−30 peaks from diffraction off either AP or NaCl. The 10−20 AP peaks observed per pattern at lower pressures were indexed as the orthorhombic P_{nma} space group according to JCPDS card 08-0451 for AP.[12] Average cell parameters (obtained from nonlinear fits to the expression for orthorhombic d spacing) were used to calculate unit cell volumes. The standard deviation of

the cell parameters was used with error propagation to estimate uncertainties of the unit cell volumes.

The mixture of AP and NaCl (in a 4:1 ratio) ground finely, was used so that the NaCl could be utilized for in situ pressure measurement. Microgram quantities of this mixture were firmly packed into each gasket hole, and flooded by placing a pipetted drop of FC-75 on the gasket hole. The cells loaded with samples and FC-75 were then quickly clamped to ensure that no air bubbles were trapped within the gasket hole. In addition to these cells, a few samples were prepared without FC-75 with only the pure 4:1 AP:NaCl mixture, to improve signal-to-noise ratio of diffraction collected above the freezing pressure of FC-75, 3.5 GPa. A single sample prepared with liquid N_2 as a pressure medium was loaded by the immersion technique.

The high-pressure cells used for X-ray diffraction were Merrill-Basset cells fabricated from 301 stainless steel. Type-IA diamond anvils purchased from Harris Diamonds Inc., were used. Each anvil weighed about 0.3 carats. The diamond culets were polished to 0.6−1 mm diameter flats. The 1 × 1 cm sized gaskets employed were cut from 0.1 mm thick stainless steel sheets and drilled with 0.3−0.6 mm diameter gasket holes. The high-pressure cell was mounted on a micrometer-positioning device for synchrotron beam alignment during X-ray diffraction measurements.

The pressure was evaluated in situ by using the NaCl diffraction peaks to calculate a unit-cell volume and applying that to pressure−volume equations of state for NaCl. The pressure reported here is the average of the values obtained from the modified Decker equation of state[13] and the Spetzler[14]-Fritz[15] EOS as analyzed by Birch,[16] for NaCl. The uncertainty of each pressure value reported is the standard deviation of the average.

IV. Results

A. Structural Studies. *1. Hydrostatic Measurements.* Infrared and Raman spectra for crystalline AP were measured as a function of pressure up to 5.0 GPa. No detectable changes were observed in the IR spectra collected below 2.9 GPa. Only broad absorptions are detected in the infrared spectrum. At ambient pressure the AP Raman spectrum is similar to that previously reported[8] and thus vibrational modes were assigned. The Raman modes were clearly resolved and an accurate determination of the pressure dependence of the detected Raman frequencies was determined. Figure 1 shows the positions of the ClO_4^- ν_2 vibration at 463 cm^{-1} and the NH_4^+ ν_1' vibrations at 3212 cm^{-1}. From ambient pressure to 0.9 GPa, the vibrational energies linearly increase with pressure, indicating uniform compression. At 0.9 GPa, a discontinuity is observed in the vibrational energy shift of the 463 mode as show in Figure 1. At the same pressure, the rate of change in energy of the 3212 mode changes. Lines connecting data points are added to Figure 1 to clarify discontinuities. The lines were determined using a linear least-squares fit to the data. The best linear least-squares fit occurs when each region is determined independent of the other pressure regions. Above 0.9 GPa, the vibrational energies increase linearly with pressure (albeit at different rates), up to a pressure of 3.0 GPa. At 3.0 GPa, a second discontinuity is observed in the 3212 vibrational mode, and the rate of energy increase of the 463 mode shows a change in slope. The second discontinuities are accompanied by the appearance of two new modes (462 and 958 cm^{-1}) as marked by arrowheads in Figure 2. Above 3.0 GPa, a monotonic increase of vibrational energies is observed up to 5.0 GPa.

Energy-dispersive X-ray diffraction (EDXD) patterns for AP were collected as a function of pressure from atmospheric pressure up to 5.0 GPa. The lattice structure of AP is orthorhombic at ambient pressure and the observed diffraction lines were indexed accordingly. Figure 3 shows selected diffraction patterns for AP as a function of pressure, obtained from the sample with only the AP:NaCl mixture, i.e., under quasi-hydrostatic pressure conditions. (Under quasi-hydrostatic pressure conditions, there is usually a small pressure gradient across the sample. Hence pressure values measured are literally an average over the X-ray-sampled cross section. Therefore, the pressure values cited here for hydrostatic conditions are slightly different from those listed in the caption of Figure 3. This is further addressed later in the Discussion Section.) The atmospheric-pressure pattern consists of the same peaks as the pattern shown in Figure 3, labeled **A**. As hydrostatic pressure is increased to above 0.9 GPa, several new diffraction lines are

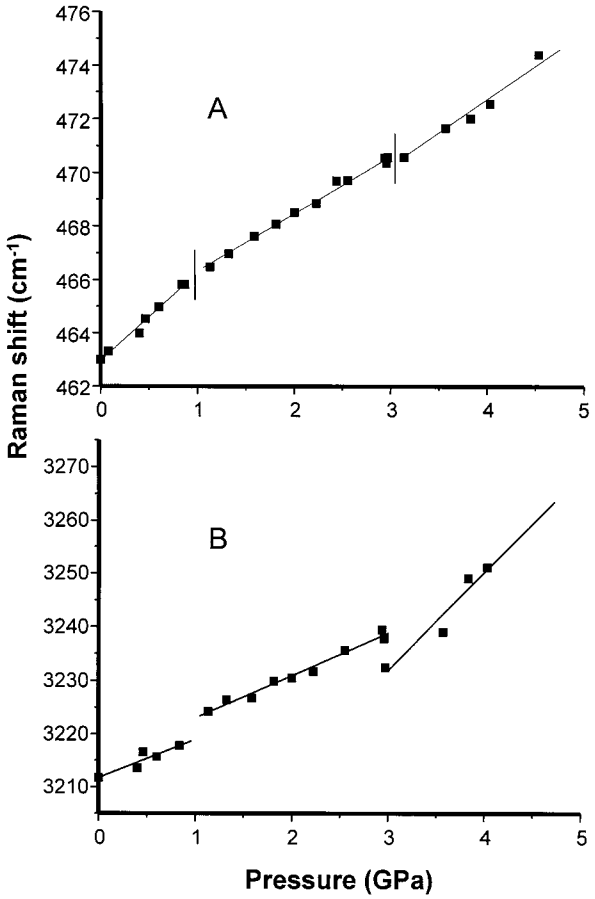

Figure 1. The shift in vibrational energy as a function of pressure for the (A) ClO_4 ν_2 vibration at 463 cm^{-1} and **(**B) the NH_4 ν_1 vibration at 3212 cm^{-1}, respectively. Vertical bars delineate regions where data points are least-squares fit with lines. Error bars for vibrational energies are within the symbol.

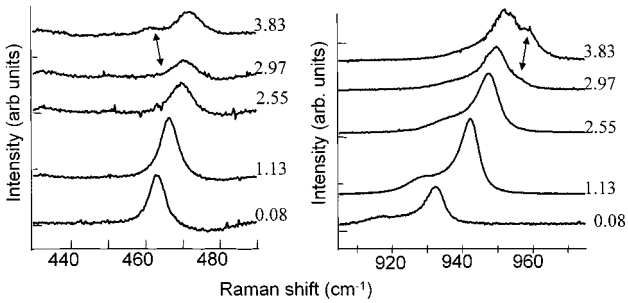

Figure 2. Pressure dependence of the ClO_4 Raman vibrations to 3.8 GPa. Black arrowheads denote the new modes appearing at 462 and 968 cm^{-1} above 2.9 GPa.

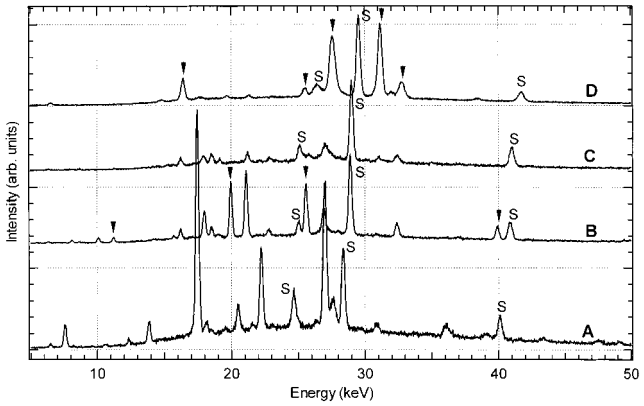

Figure 3. X-ray diffraction patterns of AP, loaded without a pressure transmitting medium, at (**A**) 1.0 GPa, (**B**) 2.9 GPa, (**C**) 3.3 GPa, and (**D**) 5.6 GPa. The arrowheads denote new peaks that appear at hydrostatic pressures above 0.9 GPa and above 3.0 GPa. The peaks marked "S" are salt (NaCl) peaks.

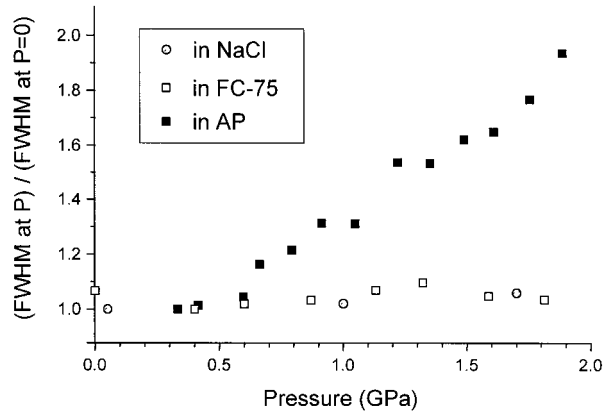

Figure 4. The fwhm of the ruby R_1 fluorescence peak at pressure in comparison to the fwhm at ambient pressure, for a ruby sphere surrounded by NaCl, FC-75, or AP and compressed to 2.0 GPa.

observed among the prevalent diffraction peaks from the orthorhombic structure. These new peaks cannot be indexed to the orthorhombic pattern, however the prevalent pattern can still be perfectly indexed to the ambient-pressure structure. From 0.9 to 2.9 GPa, the new peaks continue to gain intensity but the original diffraction peaks are present and can be indexed as the ambient structure. Black arrowheads on the **B** spectrum in Figure 3 denote the new peaks. By about 3.0 GPa the entire diffraction pattern reduces in intensity (spectrum marked **C** in Figure 3) and a new set of peaks appear. Above 3.0 GPa, all the peaks seen at lower pressure disappear completely and an entirely new pattern of peaks (not attributable to the ambient orthorhombic structure) start gaining intensity. The new pattern gains intensity to 5.6 GPa, the highest pressure used in this study. This high-pressure pattern (labeled **D** in Figure 3) consists of fewer peaks than the ambient orthorhombic phase's diffraction pattern.

2. Non-Hydrostatic Measurements. At ambient pressure AP is softer than NaCl. [See calculated EOS later in this paper.] Therefore, we expected the compression of AP to be similar to that of NaCl. NaCl is considered quasi-hydrostatic as a function of pressure up to 10.0 GPa. The width of the ruby R_1 line is a good indicator of non-hydrostaticity. Figure 4 shows a comparison of the ruby R_1 peak width (fwhm) as a function of pressure. No pressure broadening of the ruby R_1 fluorescence was observed in pure NaCl and in FC-75 to 2.0 GPa. Conducting the same experiment with AP though resulted in some interesting effects. In AP, up to 0.6 GPa, similar to NaCl and FC-75, no pressure broadening of the ruby R_1 line was observed. However, above 0.6 GPa in AP the R_1 width increases rapidly indicating a building of non-hydrostatic stress. The width of the ruby R_1 peak doubles by 2.0 GPa. Optical measurements were performed to ensure no pinching of the ruby during pressurization. Therefore this increase in the width of the ruby R_1 line must be due to the build-up of non-hydrostatic stresses, caused by mechanisms occurring within the AP surrounding the ruby chip, during compression.

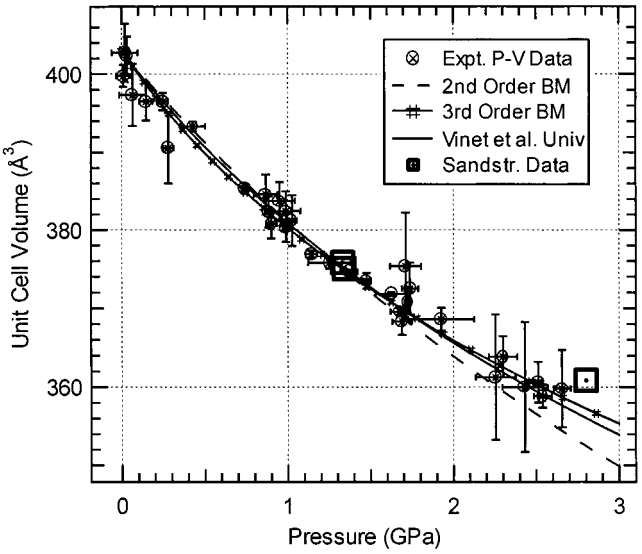

Figure 5. Volume compression of AP to 2.9 GPa, with the fitted Birch-Murnaghan (BM) and Vinet's universal equations of state. Sandstrom et al.'s data points (square symbols) were included for comparison.[7]

Raman spectra of the vibrational modes of AP were also collected with pure AP compressed to fill the gasket. Similar results were observed in the non-hydrostatic studies as reported in the hydrostatic experiments. The first discontinuity in the non-hydrostatic experiments was observed at 1.5 GPa for the 3212 cm^{-1} vibration and at 1.8 GPa for the 463 cm^{-1} vibration. The same discontinuities are observed but they are not as abrupt/anomalous as those observed under hydrostatic studies. The second discontinuity is observed at 3.3 GPa and the two new vibrations at 462 and 968 cm^{-1} were also observed.

When X-ray diffraction is obtained from samples under non-hydrostatic pressure conditions as shown Figure 3, all the phenomena listed under hydrostatic conditions are observed, though, at slightly higher-pressure ranges. (This will be discussed in the Discussion Section.) At 1.0 GPa (labeled **A** in Figure 3), the pattern is the same as expected for the ambient orthorhombic phase. Around 1.7 GPa the new peaks emerge and gain intensity to about 2.9 GPa as labeled **B** in Figure 3. Then between 2.9 and 3.3 GPa the entire spectrum loses intensity as shown in Figure 3 **C**. Above 3.3 GPa, the entire spectrum is replaced by a new pattern which gains intensity and remains stable to 5.6 GPa. This is new pattern is labeled **D** in Figure 3.

B. Isothermal Compression. The calculated unit cell volumes, from the X-ray diffraction patterns at each pressure monitored, are used to determine the isothermal compression of AP. Figure 5 highlights the isothermal compression of AP to 3.0 GPa. Notice the larger volume error bars in the data points above 1.5 GPa. These error bars could be due to slight changes in the unit cell structure because X-ray diffraction and Raman spectroscopy indicate structural changes above 0.9 GPa. However, the structural effect of these changes is apparent only in unit-cell volumes at pressures of 1.5 GPa or higher.

TABLE 1: Pressure−Volume Data Obtained from X-ray Diffraction Measurements of the Isothermal Compression of AP

run	pressure (GPa)	volume (Å^3)
101	0.07 ± 0.08	397.4 ± 4.0
104	0.02 ± 0.08	402.7 ± 3.7
111	0.28 ± 0.03	390.6 ± 4.5
112	0.43 ± 0,07	393.3 ± 0.6
113	0.95 ± 0.09	383.8 ± 2.4
115	2.30 ± 0.09	363.8 ± 2.6
116	3.20 ± 0.07	358.6 ± 5.7
201	0.01 ± 0.04	399.8 ± 1.4
202	0.15 ± 0.04	396.5 ± 2.4
204	0.74 ± 0.02	385.3 ± 0.4
205	0.88 ± 0.02	382.3 ± 2.0
206	0.90 ± 0.03	380.8 ± 1.9
207	0.99 ± 0.02	380.3 ± 1.8
209	1.14 ± 0.04	376.9 ± 0.4
210	1.25 ± 0.13	375.8 ± 0.8
213	1.63 ± 0.09	371.8 ± 0.2
214	2.54 ± 0.05	358.9 ± 1.5
401	1.48 ± 0.03	373.5 ± 1.0
403	1.69 ± 0.06	368.3 ± 1.7
404	1.72 ± 0.02	370.7 ± 1.3
405	1.93 ± 0.20	368.6 ± 1.4
406	2.66 ± 0.05	359.8 ± 4.9
501	0.25 ± 0.03	396.5 ± 1.1
502	1.37 ± 0.05	374.6 ± 0.2
503	1.68 ± 0.06	369.5 ± 0.5
504	0.87 ± 0.07	384.6 ± 2.5
505	0.99 ± 0.09	382.4 ± 2.6
507	1.71 ± 0.09	375.3 ± 6.9
508	2.25 ± 0.12	361.2 ± 7.9
509	2.43 ± 0.14	360.0 ± 8.2
601	0.03 ± 0.01	402.4 ± 2.4
603	1.03 ± 0.03	381.2 ± 3.3
604	1.74 ± 0.05	372.5 ± 3.3
605	2.92 ± 0.03	348.0 ± 4.5
606	3.32 ± 0.04	350.5 ± 0.1
701	2.51 ± 0.02	360.6 ± 2.6

Table 1 lists the P−V data obtained. Compression was measured by calculating V/V_0, where $V_0 = 403$ Å^3. Elastic parameters were calculated by fitting both the Birch-Murnaghan (BM),[16] and Vinet et al.'s Universal (VU),[17] equations of state (EOS) to the data. Initially, only the P−V data to 0.9 GPa was used because certain structural changes are observed at this pressure and the exact AP unit cell above 0.9 GPa has not been accurately estimated at this time. To 0.9 GPa, the second-order BM equation of state yields a zero-pressure isothermal bulk modulus (K_0) of 15.2 ± 0.3 GPa, with its pressure derivative constrained to 4.0. The third-order BM EOS gives a bulk modulus of 12.2 ± 1.3 GPa, with a pressure derivative (K_0') of 12.1 ± 3.5. The VU EOS yields a bulk modulus of 12.9 ± 1.9 with a derivative of 9.9 ± 4.9. Subsequently, data to 2.9 GPa was used to obtain these parameters. Then the second-order BM EOS yields a K_0 of 16.0 ± 0.2, and the third-order yields a K_0 12.7 ± 0.7, with a K_0' of 11.0 ± 1.6. To 2.9 GPa the VU EOS yields a K_0 13.5 ± 0.9, with a K_0' of 9.1 ± 1.7. The values obtained to 2.9 GPa are more precise than those obtained to 0.9 GPa because there are more data points and the fits are statistically better.

V. Discussion

Considering the hydrostatic and non-hydrostatic studies described above structural changes in AP are detected starting around 0.9 GPa. The ruby peak widths in Figure 4 seem to indicate that this structural change is related to a non-hydrostatic response of AP to stress starting at 0.6 GPa. Additionally, ammonium salts have low barriers to rotation of NH_4 ions, and NH_4ClO_4 in particular, is known to have nearly free-rotating ammonium ions at room temperature.[5,18,19] Increased pressure probably "freezes" or slows the rotating motions of the NH_4 molecular components, similar to the quenching observed upon cooling to 10 K.[5] Such freezing at pressure would not change the entire lattice symmetry but simply limit or reduce the motion of the NH_4 ions, concentrating electron density within the NH_4 molecular units in particular directions or orientations. The NH_4 molecular units would thereby lose some local site symmetry. The loss of local site symmetry may result in a few additional diffraction peaks as we observed at and above 0.9 GPa. Moreover, the orientations of the NH_4 ions would be governed by hydrogen-bonding forces between different molecules, causing the lattice to be non-hydrostatic when compressed as observed by the width of the ruby lines. However, none of this would change the positioning of NH_4ClO_4 molecules in the lattice and therefore, would not change the original orthorhombic symmetry at this pressure. Sandstrom et al. using X-ray diffraction could not observe this transition probably because their data is taken at large pressure intervals.[7] Brill and Goetz using infrared vibrational spectroscopy does report a transition in this pressure range. However, they are unable to characterize it due to low-resolution IR signals that were too broad.[8]

From 0.9 to 2.9 GPa, the original diffraction peaks are present and can be indexed as the ambient-pressure lattice structure. However, a continual gain in intensity of all the new diffraction peaks is observed. This may indicate the continued freezing and directional orientation of NH_4 ions. Therefore, between 0.9 and 2.9 GPa, AP consists of a mixture of NH_4 ions of different local symmetry with different strengths of hydrogen-bonding between molecules. It is possible that this structure could be explained with an "expanded" orthorhombic unit cell composed of more molecules within the unit cell, or still other structural descriptions may exist that fit our X-ray and Raman observations. Further studies using a high-pressure single crystal X-ray diffraction technique between 0.9 and 2.9 GPa are currently being performed to help clarify the structure of AP in this pressure region.

Between 2.9 and 3.0 GPa, the entire diffraction pattern (the ambient pattern peaks and the new ones that emerged at 0.9 GPa) loses intensity. Compression beyond 3.0 GPa results in the emergence of several peaks in new locations with widely differing *d* spacing, denoting an entirely new diffraction pattern. Considering the positions and intensities of the observed "new" diffraction pattern, it is easy to see that this high-pressure structure is entirely different to the ambient pressure structure. The diffraction pattern of this high-pressure phase continues to gain intensity to the highest pressure of 5.6 GPa used in this study. The driving force of this phase transition is probably the increased hydrogen-bonding between molecules that allow a tighter packed lattice. However the unit-cell lengths *a*, *b*, and *c*, compress similarly with pressure and it is not possible to predict a structure based on extent of compression in a particular direction.

Considering the Raman spectra, at 3.0 GPa, a second discontinuity in the pressure dependence of Raman vibrations is accompanied by the appearance of two new Raman modes. Since the ClO_4 and NH_4 vibrational modes are still observed above 3.0 GPa, the higher-pressure phase still contains the perchlorate and ammonia molecular units. The positions of the new Raman peaks being close in energy to (almost like shoulders to current peaks) the existing peaks may indicate that there are now two or three different types of ammonia or perchlorate units each with slightly different bonding within the

unit. The corresponding X-ray diffraction pattern at and above this pressure clearly indicates a new phase transition to different lattice symmetry. Bridgman too reports a cusp-like maximum at 3.1 GPa, probably due to this phase transition.[6] Sandstrom has observed this transition above 3.57 GPa.[7] We observe the onset of this new phase at 2.9 GPa, and record fewer diffraction peaks than the ambient-pressure X-ray pattern. Therefore, we speculate that this phase is of higher symmetry than the orthorhombic phase. This phase is stable to 5.6 GPa, the highest pressure used in this study.

Similar results are observed under non-hydrostatic conditions. However, it is more difficult to discern transition pressures and subtle changes, which are detected under hydrostatic conditions. This is probably do to a pressure gradient across the sample, which effectively gives pressure-averaged measurements. Consider a ruby chip in the center of a gasket hole filled with sample. When a large pressure gradient is present (non-hydrostatic), the minimum pressure over the entire region has to be at least the transition pressure (P_{trans}). Hence, the measured pressure in the center has to be higher than the transition pressure. Similarly, when NaCl is mixed with AP, and used as a pressure-measuring tool in our diffraction experiments, the entire area sampled by the synchrotron beam (approximately 0.1 mm diameter) should retain at least P_{trans}. Therefore, when a pressure medium is not used and higher-pressure gradients are present, the average pressure calculated from NaCl may be higher than P_{trans}. Thus, samples compressed non-hydrostatically show higher transition pressures than those compressed with a pressure-transmitting medium.

The P−V isothermal compression plots also show larger volume error bars above 1.5 GPa. These error bars probably demonstrate the effect of subtle structural or molecular changes indicated by the Raman spectroscopy and the X-ray diffraction above 0.9 GPa. The unit cell defined by the ambient-pressure local symmetry (within the orthorhombic lattice) may need redefining to accommodate the new local symmetry. The exact unit cell above 0.9 GPa has not yet been accurately estimated. Therefore, even though the EOS parameters obtained to 2.9 GPa are more precise than those obtained to 0.9 GPa, physically, the more accurate estimate of the bulk modulus of AP should use data below 0.9 GPa. In those EOS fits to data below 0.9 GPa, the third-order BM and VU EOS yield rather a wide range of K_0' (12.1 and 9.9, respectively) suggesting that the best formalism for these data in this pressure range is the second-order BM EOS. Therefore, the best value for the zero-pressure isothermal bulk modulus of AP is 15.2 ± 0.3 GPa, with a fixed pressure derivative of 4.0.

VI. Conclusions

AP exhibits several phase transitions as a function of pressure. The first transition is at about 0.9 GPa, where new X-ray diffraction peaks appear without much change in the ambient-pressure pattern. At about the same pressure, discontinuities are observed in the vibrational energies with pressure or in the rate of increase in vibrational energies with pressure. This first transition is tentatively identified as the freezing of hereto free-rotating NH_4 ions in the AP lattice. Between 0.9 and 2.9 GPa the new diffraction peaks increase in intensity while the ambient-pressure pattern can still be indexed.

The second phase transformation in AP is observed at 3.0 GPa and demonstrated by a second set of discontinuities in certain Raman frequencies and the appearance of two new vibrational modes. X-ray diffraction studies show an entirely new diffraction pattern at this pressure. The new pattern consists of fewer peaks than the orthorhombic pattern, possibly implying that the new structure is of higher lattice symmetry than the orthorhombic ambient structure.

The observation of two transitions in AP between ambient and 5.0 GPa, clarify the inconsistency among previous reports of pressure-induced phase transitions in AP at room temperature. Clearly, Brill and Goetz using vibrational spectroscopy identified the transition at 0.9 GPa, while Bridgeman and subsequently Sandstrom et al. observed the second transition at 3.0 GPa. The character of the first transition reported in this paper is also in keeping with the low-temperature behavior of AP where the "freezing" of freely rotating NH_4 units has been observed before. Further, similar to low-temperature studies, extended freezing leads to the generation of strong hydrogen-bonds which then drive the second transition to a phase with new lattice symmetry.

Finally, the pressure−volume data obtained were used to calculate an accurate equation of state for the isothermal compression of AP. Data to 0.9 and 2.9 GPa, respectively, were fitted with both Birch-Murnaghan and Vinet's universal equations of state formalisms. Even though the data to 2.9 GPa give statistically better fits, as possible subtle structural changes are observed above 0.9 GPa, only data to that pressure should be used to estimate thermodynamic parameters for the ambient pressure phase. Hence we report the zero-pressure isothermal bulk modulus of AP to be 15.2 ± 0.3 GPa with a pressure derivative constrained to 4.0.

Acknowledgment. The Naval Research Laboratory and the Office of Naval Research supported this work. A part of this work is based upon research conducted at the Cornell High Energy Synchrotron Source (CHESS) which is supported by NSF under award DMR 97-13424. We acknowledge the friendly assistance of all CHESS staff, specifically B1 beamline operator Chang-Sheng Zha.

References and Notes

(1) Brill, T. B.; Budenz, B. T. *Progress in Aeronautics and Astronautics*, Vol. 185; Yang, V., Brill, T. B., Ren, W. Z., Eds.; American Institute of Aeronautics and Astronautics, 2000; Chapter 1.1, Solid Propellant Chemistry, Combustion and Motor Interior Ballistics, pp 3−32.

(2) Parsonage, N. C.; Stavely, L. A. K. *Disorder in Crystals*; Clarendon Press: Oxford, England, 1978.

(3) Stammler, M.; Bruenner, R.; Schmidt, W.; Orcutt, D. *Adv. X-ray Anal.* **1976**, *9*, 170.

(4) Jacobs, P. W. M.; Russell-Jones, A. *J. Phys. Chem.* **1968**, *72*, 202.

(5) Chakraborty, T.; Khatri, S. S.; Verma, A. L. *J. Chem. Phys*. **1986**, *84*, 7018.

(6) Bridgman, P. W. *Proc. Am. Acad. Arts Sci.* **1937**, *72*, 45.

(7) Sandstrom, F. W.; Persson, P. A.; Olinger, B. Isothermal and shock compression of high-density ammonium nitrate and ammonium perchlorate. *10th Detonation Symposium*; Boston, MA, Office of Naval Research, 1995; pp 766−774.

(8) Brill, T. B.; Goetz, F. Laser Raman studies of solid oxidizer behavior. *Papers in Aeronautics and Astronautics*, Vol. 63; Boggs, T. L., Zinn, B. T., Eds.; American Institute of Aeronautics and Astronautics, 1978; pp 3−19.

(9) Foltz, F. M.; Maienschein, J. L. *Mater.Lett.* **1995**, *24*, 407.

(10) Russell, T. P.; Piermarini, G. J. *J. Rev. Sci. Instrum.* **1997**, *68*, 1835.

(11) Piermarini, G. J.; et al. *Appl. Phys*. **1975**, *46*, 2774.

(12) Joint Committee on Powder Diffraction Standards currently named International Center for Diffraction Data.

(13) Decker, D. L.; et al. *J. Phys. Chem. Ref. Data* **1972**, *1*, 773.

(14) Spetzler, H.; Sammis, C. G.; O'Connell, R. J. *J. Phys. Chem. Solids* **1972**, *33*, 1727.

(15) Fritz, J. N.; et al. *Nat. Bur. Stand. U.S. Spec. Publ*. **1971**, *326*, 201.

(16) Birch, F. *J. Geophys. Res*. **1978**, *83*, 1257.

(17) Vinet, P.; Ferrante, J.; Smith, J. R.; Rose, J. H. *J. Phys. C: Solid State Phys.* **1986**, *19*, L467.

(18) Leung, P. S.; Rush, J. J.; Taylor, T. I. *J. Chem. Phys*. **1972**, *57*, 175.

(19) Corn, R. M.; Strauss, H. L. *J. Chem. Phys*. **1983**, *79*, 2641.